

# The impact of spatiotemporal structure of rainfall on flood frequency over a small urban watershed: an approach coupling stochastic storm transposition and hydrologic modeling

Zhengzheng Zhou<sup>1</sup>, James A. Smith<sup>2</sup>, Mary Lynn Baeck<sup>2</sup>, Daniel B. Wright<sup>3</sup>, Brianne K. Smith<sup>4</sup>, Shuguang Liu<sup>1</sup>

<sup>1</sup>Department of Hydraulic Engineering, Tongji University, Shanghai, China.

<sup>2</sup>Department of Civil and Environmental Engineering, Princeton University, USA.

<sup>3</sup>Department of Civil and Environmental Engineering, University of Wisconsin-Madison, USA.

<sup>4</sup>Department of Earth and Environmental Sciences, City University of New York-Brooklyn College, USA.

Corresponding to: Zhengzheng Zhou (19058@tongji.edu.cn); Shuguang Liu ([liusgliu@tongji.edu.cn](mailto:liusgliu@tongji.edu.cn))

**Abstract.** The role of rainfall space-time structure, as well as its complex interactions with land surface properties, in flood response remains an open research issue. This study contributes to this understanding, specifically for small (<15 km<sup>2</sup>) urban watersheds. Using a flood frequency analysis framework that combines stochastic storm transposition-based (SST) rainfall scenarios with the physically-based distributed GSSHA model, we examine the role of rainfall spatial and temporal variability in flood frequency across drainage basin scales in the highly-urbanized Dead Run watershed (14.3 km<sup>2</sup>), Maryland, USA. The results show the complexities of flood response within several subwatersheds for both short (<50 years) and long (>100 years) rainfall return periods. The impact of impervious area on flood response decreases with increasing rainfall return period. For extreme storms, the maximum discharge is closely linked to the spatial structure of rainfall, especially storm core spatial coverage. The spatial heterogeneity of rainfall increases flood peak magnitudes by 50% on average at the watershed outlet and its subwatersheds for both small and large return periods. The framework of SST-GSSHA-coupled frequency analysis also highlights that spatially distributed rainfall scenarios are needed in quick-response flood frequency even for relatively small basin scales.

## 1. Introduction

Rainfall spatiotemporal structure plays an important role in flood generation in urban watersheds (Saghafian *et al.*, 1995; Smith *et al.*, 2005b; Emmanuel *et al.*, 2012; Nikolopoulos *et al.*, 2014). Spatial heterogeneities in land use and land cover complicate the translation of rainfall spatiotemporal distribution into flood responses (Galster *et al.*, 2006; Morin *et al.*, 2006; Ntelekos *et al.*, 2008; Ogden *et al.*, 2011; Yin *et al.*, 2016; ten Veldhuis *et al.*, 2018), especially for small catchments (Faurès *et al.*, 1995; Smith *et al.*, 2005a; Zhou *et al.*, 2017; Zhou *et al.*, 2019; Yang *et al.*, 2020). The influence of rainfall

31 spatial-temporal structure on flood frequency analysis in urban areas remains an open research issue.

32 Previous studies have demonstrated the sensitivity of hydrological response to rainfall variability in both space and time  
33 (Smith *et al.*, 2012; Ochoa-Rodriguez *et al.*, 2015; Rafieeiniasab *et al.*, 2015). Following the advent of rainfall measurement  
34 using weather radar (Fulton *et al.*, 1998; Krajewski and Smith, 2002), many studies have highlighted the use of high-  
35 resolution rainfall data in assessing rainfall variability over various range of spatial and temporal scales (Berne *et al.*, 2004;  
36 Gebremichael and Krajewski, 2004; Moreau *et al.*, 2009; Emmanuel *et al.*, 2012) and how their use could improve runoff  
37 estimation (Morin *et al.*, 2006; Smith *et al.*, 2007; Schellart *et al.*, 2012; Wright *et al.*, 2014b; Rafieeiniasab *et al.*, 2015;  
38 Gourley *et al.*, 2017).

39 There are conflicting findings on the relative importance of rainfall temporal and spatial characteristics. Paschalis *et al.*  
40 (2014), Ochoa-Rodriguez *et al.* (2015) and Yang *et al.* (2016) found that “coarsening” temporal resolution has a stronger  
41 impact on flood response than coarsening spatial resolution. Adams *et al.* (2012) found the space-time averaging effects of  
42 routing through the catchment notably remove the impact of spatially variable rainfall at a 150-km<sup>2</sup> catchment scale. Bruni  
43 *et al.* (2015), in contrast, found a higher sensitivity of modeled flow peaks to spatial resolution rather than the temporal  
44 resolution. Peleg *et al.* (2017) showed an increasing contribution of the spatial variability of rainfall to the variability of  
45 flow discharge with longer return periods. Cristiano *et al.* (2018); Cristiano *et al.* (2019) found the spatial aggregation of  
46 rainfall data can have a strong effect on hydrological responses. Zhu *et al.* (2018) examined the influence of rainfall  
47 variability on flood frequency analysis and addressed the impact of antecedent moisture in flood generation for various  
48 basin scales.

49 Stochastic Storm Transposition (SST) was developed as a physically-based stochastic rainfall generator for rainfall  
50 frequency analysis. Previous studies show that SST with relatively short records (10 or more years) of high-resolution radar  
51 rainfall fields can produce reasonable rainfall scenarios with realistic spatial-temporal structure, which cannot be provided  
52 by conventional design storm methods. In the conventional approach, the idealized assumptions include idealized rainfall  
53 temporal structure, uniformed spatial distribution and 1:1 rainfall-flood return periods equivalence (see (Wright *et al.*, 2013;  
54 Wright *et al.*, 2017; Zhou *et al.*, 2019), and references therein). These assumptions ignore the interaction between the  
55 spatiotemporal structure of rainfall and flood response, which increases the uncertainty of frequency estimations. Coupled  
56 with hydrological models, the SST-based framework can be used for multiscale rainfall frequency analysis and flood  
57 frequency analysis that accounts for rainfall variability and surface characteristics (Wright *et al.*, 2014a; Perez *et al.*, 2019;  
58 Yu *et al.*, 2019; Wright *et al.*, 2020).

59 Previous studies have demonstrated that the relationship between rainfall and flood is scale-dependent, varying with rainfall  
60 patterns, basin characteristics, and runoff generation processes. However, there is still no clear answer on the relative

61 importance of temporal and spatial features of rainfall on flood responses (Cristiano *et al.*, 2017). Moreover, studies  
62 focusing on small (<15 km<sup>2</sup>) urbanized basins are relatively few (Peleg *et al.*, 2017) and the issues remain poorly understood.  
63 This study contributes to the understanding of the interaction between rainfall variability and flood response over small-  
64 scale urbanized watersheds (<15 km<sup>2</sup>) for a short-duration rainfall and quick hydrologic response setting. We build on the  
65 SST-based rainfall study of Zhou *et al.* (2019) using the physically-based hydrological model implementation introduced  
66 by Smith *et al.* (2015) for the Dead Run watershed outside of Baltimore, Maryland, USA. The framework of SST-based  
67 rainfall frequency analysis coupled with a hydrological model provides an effective approach for detailed flood frequency  
68 study (Wright *et al.*, 2014a; Yu *et al.*, 2019). Under the framework, we characterize the spatial and temporal features of  
69 rainfall events under different return periods and examine their roles in determining flood frequency in small urban  
70 watersheds. The following questions will be addressed: (1) How does flood frequency in small urban watersheds vary with  
71 space-time rainfall structure and rainfall magnitude? (2) What are the dominant space-time features of rainfall that control  
72 flood peak distribution in small urban watersheds? By answering the above questions, the study can improve the  
73 understanding of interactions between rainfall and flood processes in small urbanized areas. In addition, some idealized  
74 assumptions used in the conventional rainfall-flood frequency analysis will be questioned.

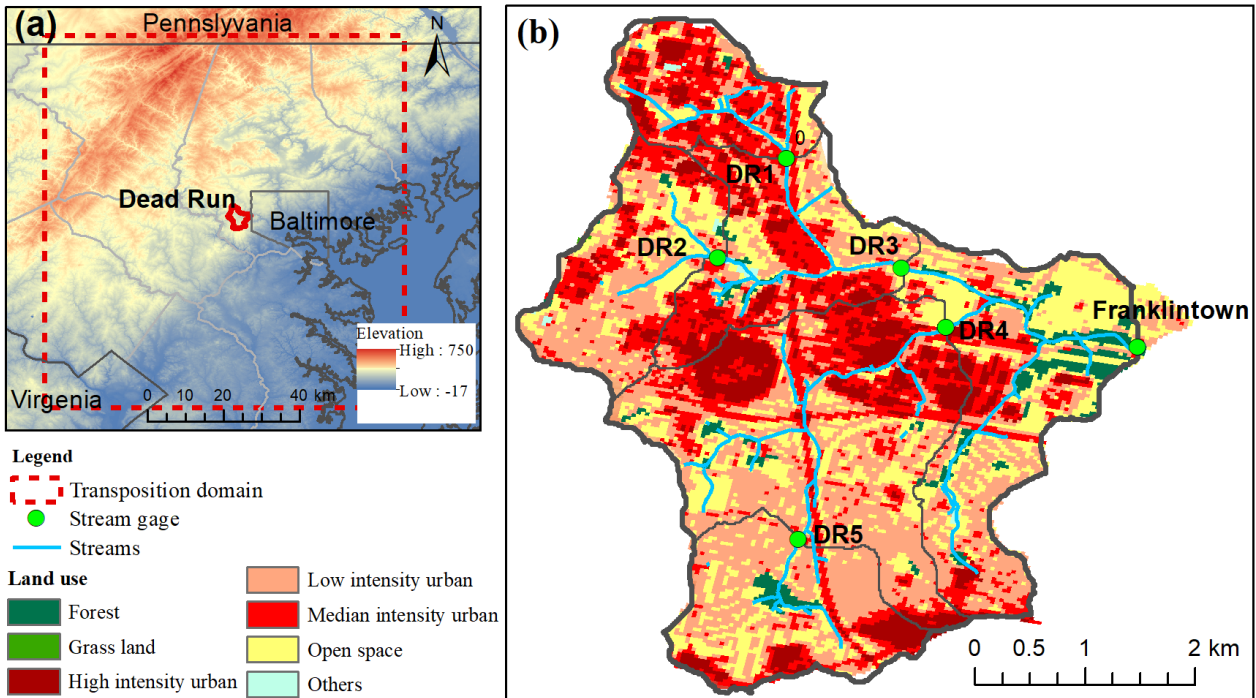
75 The paper is organized as follows. In Section 2, we introduce the study region and describe the SST-based methodology,  
76 GSSHA model, and the metrics used to characterize rainfall and flood response. In Section 3, we present model validation  
77 and analyses of flood frequency distributions and rainfall-flood relationships. A summary and conclusions are presented in  
78 Section 4.

## 79 **2. Data and method**

### 80 **2.1 Study region and data**

81 The study focuses on the highly-urbanized 14.3 km<sup>2</sup> Dead Run (DR) watershed located west of Baltimore, Maryland, USA  
82 (Fig. 1). DR is a tributary to the Gwynns Falls watershed, which is the principal study catchment of the Baltimore  
83 Ecosystem Study (BES; Pickett and Cadenasso (2006). The basin has an impervious fraction of approximately 52.3%  
84 (Table 1). The watershed has a dense network of six stream gauges with drainage areas ranging from 1.2 to 14.3 km<sup>2</sup> (Fig.  
85 1; Table 1). The subwatersheds are developed after the implementation of the Maryland Stormwater Management Act of  
86 1982 (Maryland, 1982) with many detention infrastructures such as small local ponds. The wealth of data for Dead Run  
87 provides exceptional resources to examine rainfall and hydrologic response (Beighley and Moglen, 2002; Nelson *et al.*,  
88 2006; Meierdiercks *et al.*, 2010; Smith *et al.*, 2015; Miller *et al.*, 2021). For example, Meierdiercks *et al.* (2010) analyzed  
89 the impact of storm drains and detention basins on a single storm event in DR, while Ogden *et al.* (2011) used the Gridded

90 Surface Subsurface Hydrologic Analysis (GSSHA) model to analyze the effects of storm drains, impervious area, and  
 91 drainage density on hydrologic response. Smith *et al.* (2015) created a DR model using GSSHA to examine the effects of  
 92 storage and runoff generation processes through analyses of a large number of storm events. Miller *et al.* (2021) examined  
 93 the role of stormwater management for urban flood response.



94  
 95 **Figure 1. Overview of Dead Run study region including (a) location of DR, elevation, and transposition domain of**  
 96 **SST; (b) land use land cover and stream gages. The red outline and grey outline in (a) indicates the boundary of the**  
 97 **DR watershed and Baltimore City, respectively.**

98 High resolution (15-min temporal resolution, 1-km<sup>2</sup> spatial resolution) radar rainfall fields for the 2000-2015 period were  
 99 derived from volume scan reflectivity fields from the Sterling, Virginia WSR-88D (Weather Surveillance Radar-1988  
 100 Doppler) radar. The two-dimensional radar rainfall fields are then developed from the reflectivity fields using the Hydro-  
 101 NEXRAD algorithms (Krajewski *et al.*, 2011) which have been used in rainfall and hydrological studies (Smith *et al.*, 2007;  
 102 Lin *et al.*, 2010; Smith *et al.*, 2012; Smith *et al.*, 2013; Wright *et al.*, 2014b; Zhou *et al.*, 2017). The Hydro-NEXRAD  
 103 algorithms include quality control algorithms, Z-R conversion of reflectivity to rainfall rate, time integration, and spatial  
 104 mapping algorithms (Seo *et al.*, 2011). To improve the rainfall estimates, a multiplicative mean-field bias correction (Smith  
 105 and Krajewski, 1991; Wright *et al.*, 2012) is applied on a daily basis using a network of 54 rain gauges in and around the  
 106 Baltimore County. The bias computation takes the form  $B_i = \frac{\sum S_i G_{ij}}{\sum S_i R_{ij}}$ . Where  $G_{ij}$  is the rainfall accumulation for gage  $j$  on  
 107 day  $i$ ,  $R_{ij}$  is the daily rainfall accumulation for the co-located radar pixel accumulation on day  $i$ , and  $S_i$  is the index of the  
 108 rain gage stations for which both the rain gage and the radar report positive rainfall accumulations for day  $i$ . Each 15-min

109 radar rainfall field from day  $i$  is then multiplied by  $B_i$ . The reader is directed to Zhou *et al.* (2019) and references therein  
 110 for further details on the rainfall data and bias correction methods.

111 Instantaneous discharge data with a resolution of five minutes from the U.S. Geological Survey (USGS) were used for DR-  
 112 1, DR-2, DR-5, and Franklinton. For DR-3 and DR-4, the discharge data is converted through stage-discharge curves  
 113 from Lindner and Miller (2012). Streamflow observations for the outlet station at Franklinton extend back to 1960. The  
 114 subwatersheds have records beginning in 2008.

115 **Table 1: Characteristics of the Dead Run watershed** (Smith *et al.*, 2015).

	USGS ID	Area (km <sup>2</sup> )	Developed Land <sup>a</sup> (%)	Imperviousness (%)	Detention controlled area <sup>b</sup> (%)
DR1	01589317	1.32	99%	73.6	41.9
DR2	01589316	1.92	98%	55.5	18.5
DR3	01589320	4.95	98%	62.2	24.4
DR4	01589315	6.29	98%	51.5	12.2
DR5	01589312	2.05	96%	47.9	3.2
Franklinton	01589330	14.3	96%	52.3	25.1

Note:

a. Developed lands include “Developed, open space” (>20% impervious surface), “Developed, low intensity” (20%-49% impervious surface), “Developed, medium intensity” (50%-79% impervious surface), and “Developed, high intensity” (80% or more impervious surface). Data source: USGS 2012 National Land Cover Dataset (NLCD).

b. Detention controlled area refers to the area controlled by detention infrastructure.

116

117 **2.2 GSSHA Hydrological Model**

118 The distributed physics-based GSSHA model is used to simulate multi-scale flood responses. GSSHA is a two-dimensional,  
 119 distributed-parameter raster-based (i.e. square computational cell-based) hydrologic modeling system. It uses explicit finite  
 120 difference and finite volume methods in two dimensions on a structured grid to simulate overland flow and in one dimension  
 121 to simulate channel flow (Downer and Ogden, 2004; 2006). Previous studies of the GSSHA model show that the model  
 122 with fine grid resolution can produce adequate simulations of flood response, especially when driven by high-resolution  
 123 radar rainfall fields (Sharif *et al.*, 2010; Sharif *et al.*, 2013; Wright *et al.*, 2014a; Cristiano *et al.*, 2019).

124 In this study, we use the Dead Run model created by Smith *et al.* (2015). A brief description of the model is provided here;  
 125 see Smith *et al.* (2015) for more details. The delineation of the watershed and channel network was based on a 30-m USGS  
 126 digital elevation model (Gesch *et al.*, 2002). Channel flow overland flow was set with different Manning’s roughness

127 coefficients. Additional stream channels were added based on the Baltimore County hydrography Geographic Information  
128 Systems (GIS) map. Stream cross sections were extracted from a 1-m resolution topography data set for Dead Run  
129 developed from lidar. Storm sewers in DR-2 and DR-5 were added using the Baltimore County Stormwater Management  
130 GIS map and digitized storm sewer maps. The semicircle's diameter was set to the pipe diameter. Detention basins were  
131 represented within the channel with cross sections extracted from the 1-m lidar topographic data.  
132 Several aspects of the model were modified from those used in Smith *et al.* (2015), primarily to improve computational  
133 speed. Infiltration is calculated using Richards' equation (RE) in Smith *et al.* (2015), while this study uses the three-layer  
134 Green-Ampt (GA) scheme. A uniform Manning's roughness coefficient of 0.01 is set for all the stream channels for model  
135 simplification. Initial soil moisture is approximated to be one-third of field capacity for each storm event.

### 136 **2.3 SST procedure**

137 The rainfall scenarios in this study are developed using RainyDay, an open-source SST software package (Wright *et al.*,  
138 2017). The steps used are briefly summarized here; the reader is directed to Zhou *et al.* (2019) and references therein for  
139 further details.

140 The first step is to identify a geospatial "transposition domain" that contains the watershed of interest. In this study, we use  
141 a square 7,000 km<sup>2</sup> transposition domain centered on the DR watershed. Zhou *et al.* (2019) presented a detailed examination  
142 of heterogeneity in extreme rainfall over the transposition domain using a variety of metrics, including storm counts, mean  
143 storm depths and intensities, convective activity indicated by lightning observations, and analysis of spatial and temporal  
144 rainfall structure.

145 The second step is to identify the largest  $m$  storms within the domain at the  $t$ -hr time scale. This collection of storms is  
146 referred to as a storm catalog. The storms are selected with respect to the size, shape and orientation of the DR watershed.  
147 We henceforth refer to these as "DR-shaped storms." The  $m$  DR-shaped storms are selected from an  $n$ -year rainfall record,  
148 such that an average of  $\lambda=m/n$  storms per record year is included in the storm catalog. In this study, we chose  $m = 200$   
149 storms over the 16-year radar record.

150 The third step is to randomly sample a subset of  $k$  storms from the storm catalog, where  $k$  refers to a stochastic number of  
151 storms per year. The  $k$  is assumed to follow a Poisson-distributed number of storm occurrences with rate parameter  $\lambda=m/n$   
152 storms per year. All rainfall fields associated with a storm are transposed by an east-west distance  $\Delta x$  and a north-south  
153 distance  $\Delta y$ , where  $\Delta x$  and  $\Delta y$  are drawn from distributions  $D_X(x)$  and  $D_Y(y)$  which are bounded by the limits of the  
154 transposition domain. Based on the spatial heterogeneity analysis of extreme rainfall in the domain, distributions  $D_X(x)$  and  
155  $D_Y(y)$  can be set as uniform or non-uniform. In Zhou *et al.* (2019) and this study, since the assumption of regional

156 homogeneity cannot be relaxed, we used the non-uniform distribution. A two-dimensional probability density function  
 157 (PDF) of spatial storm occurrence (Wright *et al.*, 2017) is used as the basis for non-uniform spatial transposition (Fig. A1  
 158 in Appendix A). This step can be understood as generating a “synthetic year” of extreme rainfall events over the domain  
 159 based on resampling and transposing observations. For each of the  $k$  transposed storms, compute the  $t$ -hr basin-average  
 160 rainfall depth over the watershed. Among the  $k$  rainfall depths, the maximum depth is retained as a synthetic  $t$ -hr annual  
 161 rainfall maximum for the watershed, while the transposed rainfall fields are saved for use as inputs to a GSSHA model  
 162 simulation.

163 The fourth step repeats Step 3  $S$  times to recreate multiple years of synthetic  $t$ -hour “annual” rainfall maxima and associated  
 164 transposed rainfall fields for the watershed. In this study, these steps are repeated  $S = 300$  times and the ordered “annual”  
 165 maxima are used to generate rainfall return period estimates up to 200 years. 300 such realizations of 200-yr series are  
 166 generated, and the median value of 300 realizations is used to generate estimates for return periods up to 200 years.

## 167 **2.4 Characteristics of rainfall and hydrologic response**

### 168 **2.4.1 Spatio-temporal characteristics of rainfall**

169 Rainfall statistics were computed for each event, based on radar rainfall data at 15-min, 1-km<sup>2</sup> resolution, to characterize  
 170 the spatial and temporal variability of rainfall (following Smith *et al.* (2002); Smith *et al.* (2005b); see also Zoccatelli *et al.*  
 171 (2011) and Emmanuel *et al.* (2015)). The basin-average rainfall rate (mm/h) at time  $t$  during the storm is given by:

$$172 \quad M(t) = \int_A R(t, x) dx \quad (1)$$

173 Where  $A$  is the drainage area (km<sup>2</sup>),  $R(t, x)$  is the rain rate (mm/h) at radar grid  $x$  at time  $t$ , and  $T$  (h) is the time period of  
 174 rainfall event. Peak basin-average rainfall rate (mm/h) is denoted:

$$175 \quad M_{max} = \max\{M(t); t \in [0, T]\} \quad (2)$$

176 and storm total rainfall depth (mm) is:

$$177 \quad R_{sum} = \sum_0^T M(t) \quad (3)$$

178 To characterize the spatial properties of rainfall, several dimensionless quantities are computed. Fractional coverage of  
 179 storm core at  $t$  is given by:

$$180 \quad Z(t) = \frac{1}{A} \int_A I_{(R(t,x))} dx \quad (4)$$

181 where  $I_{(R(t,x))}$  is the indicator function and equals 1 when  $R(t, x) > 25 \text{ mm/h}$  or 0 otherwise.

182 Rainfall location is given by:

$$183 \quad L(t) = \int_A \omega(t, x) d(x) dx \quad (5)$$

184 where  $\omega(t, x) = \frac{R(t, x)}{\int_A R(t, x) dx}$ ,  $d(x)$  is the linear distance from point  $x$  to the outlet. The rainfall-weighted flow distance is:

$$185 \quad \text{RWD}(t) = \int_A \omega(t, x) d_f(x) dx \quad (6)$$

186 where distance function  $d_f(x)$  is the flow distance between point  $x$  and the outlet. It is calculated as the sum of the  
187 overland flow distance from  $x$  to the nearest channel and the distance along the channel to the basin outlet. The flow distance  
188  $d_f(x)$  is normalized by the maximum flow distance, ranging from 0 to 1. RWD with values close to 0 indicates that rainfall  
189 is distributed near the basin outlet; with values close to 1 indicates rainfall concentrated at the far periphery of the basin.

190 For a uniformly distributed rainfall, the mean RWD is:

$$191 \quad \overline{\text{RWD}} = \int_A d_f(x) dx \quad (7)$$

192 The dispersion of RWD:

$$193 \quad S(t) = \frac{1}{\bar{s}} \int_A \omega(t, x) [d_f(x) - \bar{d}]^2 dx \quad (8)$$

194 where  $\bar{s} = \int_A [d_f(x) - \bar{d}]^2 dx$ ,  $S$  is a spatial indicator with values  $< 1$  indicates that rainfall is a unimodal distribution, that  
195 is, spatially one peak over the watershed;  $S$  with values  $> 1$  indicates that rainfall is a multimodal distribution.

196 The Eqs.1-3 are typical rainfall characteristics used in conventional rainfall-flood analysis since they reflect the general  
197 information of rainfall. Since the basin-averaged index will ignore the potential spatial heterogeneity over the watershed,  
198 Eqs. 4-8 describe the spatial distribution of rainfall within the area.

#### 199 **2.4.2 Spatiotemporal characteristics of hydrologic response**

200 Flood peak ( $Q_{peak}$ , mm<sup>3</sup>/s), total runoff ( $Q_{sum}$ , mm), and lag time ( $T_{lag}$ , min) are defined as:

$$201 \quad Q_{peak} = \max\{Q(t); t \in T_d\} \quad (9)$$

$$202 \quad Q_{sum} = \sum_0^{T_d} Q(t) \quad (10)$$

$$203 \quad T_{lag} = T_{Fpeak} - T_{Rpeak} \quad (11)$$

204 Respectively, where  $Q(t)$  is the flow discharge at time  $t$ ;  $T_d$  is the duration of hydrological response, which is from the  
205 start of rainfall event to the time when  $f(t) < 0.05 * Q_{peak}$ .



## 206 **3. Results and Discussion**

### 207 **3.1 Model validation**

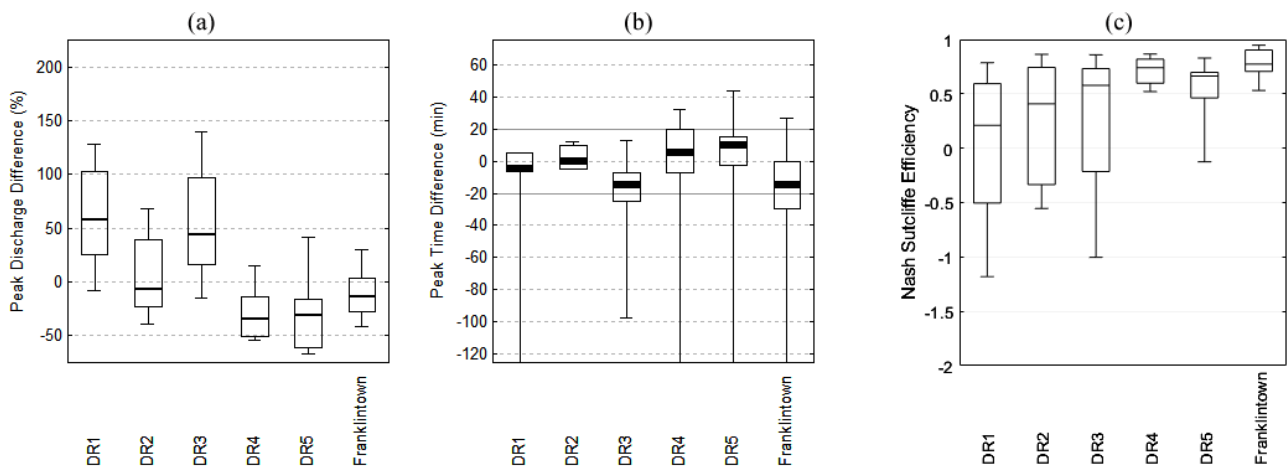
208 We validated the Dead Run GSSHA model through analyses of the 21 largest warm season (April-September) flood events  
209 with peak discharges ranging from 70.3 to 253 m<sup>3</sup>/s in the 2008-2012 period. The simulated discharge was compared to  
210 USGS streamflow observations for all six gaging stations. We assessed peak discharge, peak time and Nash-Sutcliffe  
211 Efficiency (NSE) (Nash and Sutcliffe, 1970) to examine the performance of the model.

212 Peak discharge difference is calculated as the difference between the modeled peak and measured peak as a percentage of  
213 the measured peak (Fig. 2a). The peak discharge is underestimated at DR2, DR4, DR5 and Franklinton. The median peak  
214 discharge difference at the downstream Franklinton gage was -14%. For the subwatersheds, the modeled peak at DR2  
215 matches observation best with a median difference of -7.8%. This represents relatively good performance in reproducing  
216 peak discharges for such a large collection of flood events with various peak discharges ranging from 70 m<sup>3</sup>/s to 253 m<sup>3</sup>/s.

217 The peaks at DR1 are overestimated substantially by 57% on average. The issue at DR1 was shown before in Smith *et al.*  
218 (2015) who speculate that the watershed contains a large land area that is not represented fully on county storm sewer maps.

219 The peak time difference is calculated as the time difference between the simulated peak time and measured peak time (Fig.  
220 2b). The median difference ranges from -15 min to +10 min, which is within the temporal resolution of the data (15 min  
221 for rainfall; 5 min for streamflow). It should be noted that there are several large peak time differences that occurred within  
222 the 21 storm events. These are due to the storms that produce multiple discharge peaks. The measured discharge may have  
223 the first peak as the largest while the modeled discharge has the next peak as the largest which is hundreds of minutes later.  
224 Nonetheless, the figure shows that the timing of the peak flow is well captured by the model.

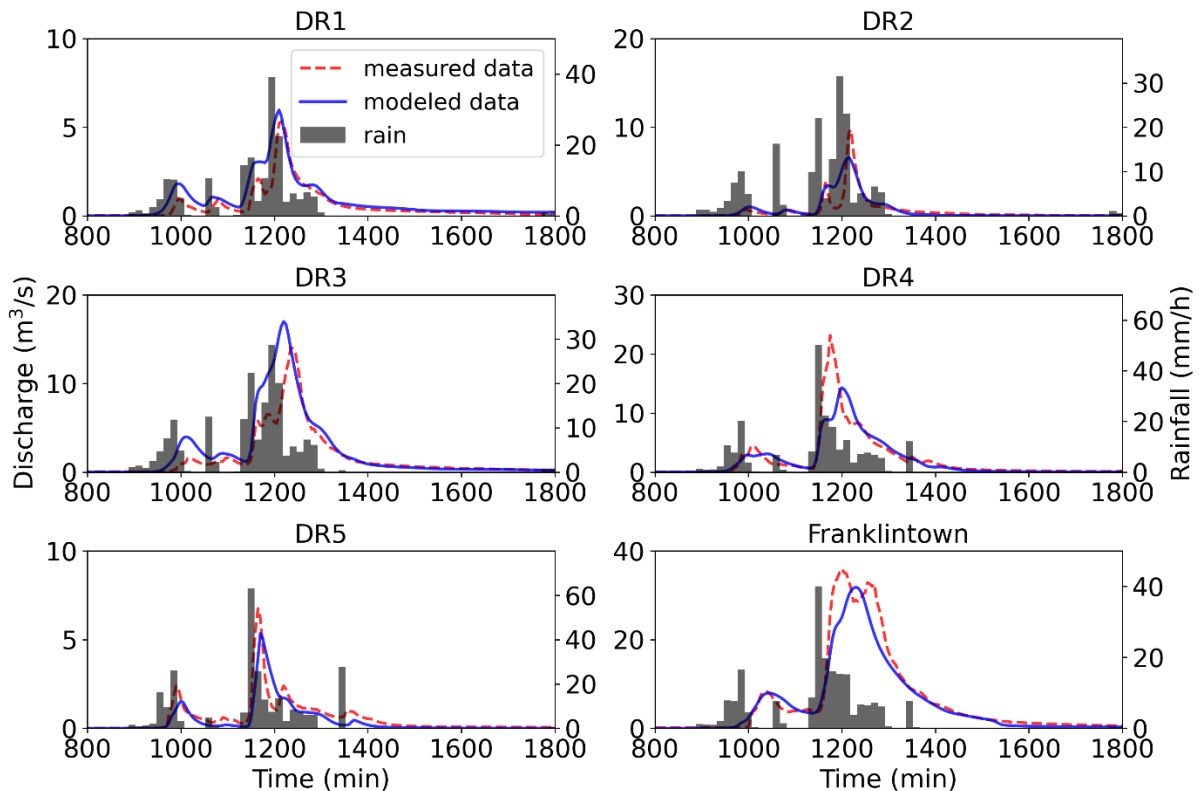
225 The median Nash-Sutcliffe Efficiency (NSE) for the 21 events at Franklinton is 0.77 (Fig. 2c). The best NSE at  
226 Franklinton is 0.97 indicating that the match between model and measured data was nearly exact. For the subwatersheds,  
227 the best median NSE is at DR-4 with a value of 0.74, while the least median NSE is at DR-1 with a value of 0.21. The  
228 results show that the main tendency of flood response is captured by the model.



229

230 **Figure 2. Comparison of (a) flood peak discharges, (b) response times and (c) NSE for 21 historical rainfall events.**

231 The hydrograph of the 14 August 2011 storm event is shown as a representative of flood simulations for the 21 events. The  
 232 peak discharge difference is -12% at Franklinton with an NSE of 0.93. Modeled hydrographs match the measured data  
 233 well at the outlet of the watershed. For the subwatersheds, the peak discharge difference ranges from -38% at DR4 to 12%  
 234 at DR-1. The shape and timing of the modeled response are similar to the measured hydrograph. But the peak discharge is  
 235 underestimated by more than 30% at DR-4.



236

237 **Figure 3. Hydrographs and rainfall for the 14 August 2011 storm event. Time refers to minutes from the start of the**  
 238 **model simulation.**

239 It should be noted that the error in simulated response may be attributable to measurement errors tied to stage-discharge  
240 curves and conversions of radar reflectivity to rainfall rate, as well as to the features that were simplified within the model,  
241 such as initial soil moisture and some aspects of the storm drain network (Smith *et al.*, 2015). For example, it has been  
242 documented that the average error of discharge between USGS direct measurements and stage-discharge curves for  
243 Franklinton is 17.4% between 2008 and 2010 (Lindner and Miller, 2012); this error likely grows for high flow conditions.  
244 Furthermore, for the rainfall data set used in this study, the median difference of the storm total rainfall between a rain gage  
245 and the bias-corrected radar rainfall data for all the pixel of gages over the 21 storms is 22.6% (Smith *et al.*, 2015). It may  
246 also increase the error in the measurements and modeling results.

247 Overall, the validation shows that the hydrological model can capture the main shape and timing of the measured response  
248 in Dead Run. We, therefore, conclude that the model is suitable for the subsequent flood frequency analysis.

### 249 **3.2 Flood frequency distribution**

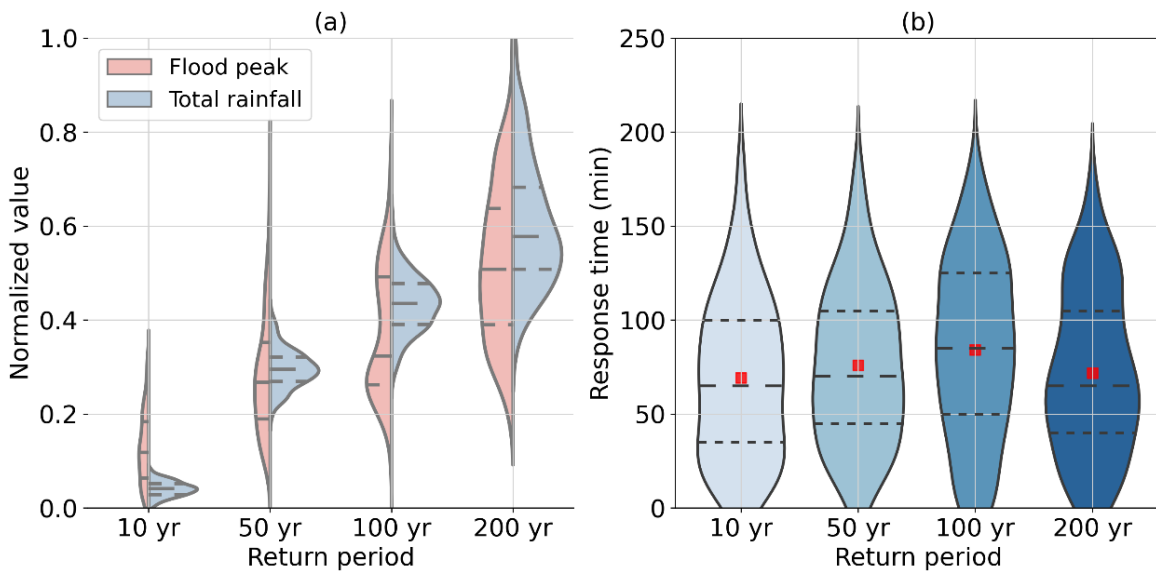
250 Under the SST framework, 3-h rainfall scenarios for 10-yr, 50-yr, 100-yr and 200-yr return periods were generated (Fig.  
251 A2 in Appendix A). For each rainfall return period, 300 realizations of rainfall events are used as input to drive the  
252 hydrological model. Henceforth, for each rainfall return period, 300 flood responses can be simulated for Franklinton and  
253 the five DR subwatersheds.

#### 254 **3.2.1 Flow discharge estimates**

255 The distribution of maximum discharge at the Franklinton gage for rainfall return periods ranging from 10 to 200 years  
256 is illustrated in Fig. 4a. To compare the distributions of rainfall and flood peaks, the values are normalized to range from 0  
257 to 1. The normalization is the ratio of values minus the minimum to the maximum minus minimum. The most striking  
258 feature is that the distributions of total rainfall and flood peaks are highly variable across the four return periods. The kernel  
259 density distribution of rainfall shows a peak at the position of 50<sup>th</sup> quantile for four return periods. The distribution of flood  
260 peaks is more complex. For the 100-yr rainfall return period, the kernel density distribution of flood peaks shows a  
261 multimodal trend with two small peaks around the 25<sup>th</sup> and 75<sup>th</sup> quantiles, which contrasts with the unimodal distribution  
262 of rainfall. The following results will show that flood peak is highly related to spatial rainfall features, implying that the  
263 multimodal distribution of flood peaks is associated with the spatial distribution of rainfall. The pronounced difference in  
264 the distributions of total rainfall and flood peaks highlights the complex relationship between rainfall properties and flood  
265 response in this relatively small urbanized watershed.

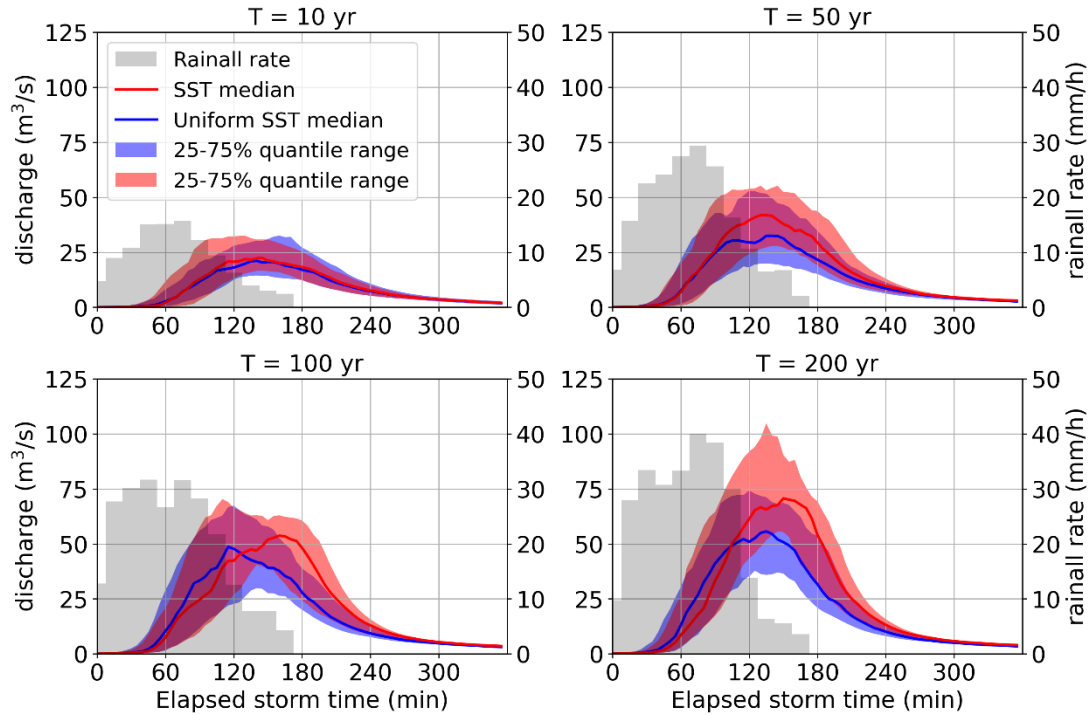
266 The flood response time is calculated as the difference between the time of maximum rainfall rate and maximum discharge

267 (Fig. 4b). Median values of response time are similar under all return periods, ranging from 70 to 83 minutes, which, given  
 268 the temporal resolution of rainfall is 15 minutes, can be similar for all four return periods. It can be concluded that although  
 269 the flood peak magnitude increases with rainfall return period, the response time is consistent for various rainfall scenarios.  
 270 This implies in this small highly urbanized watershed the response time is more linked to the drainage system rather than  
 271 to rainfall characteristics.



272  
 273 **Figure 4. Violin plots of (a) normalized flood peak and normalized total rainfall; and (b) response time from 10-y to**  
 274 **200-y rainfall return periods. (The red dot indicates the mean value. The dashed line in the middle indicates the**  
 275 **median value. Upper and lower dashed lines indicate the 75<sup>th</sup> and 25<sup>th</sup> quantiles, respectively.) The rainfall return**  
 276 **periods are calculated with respect to the average rainfall rate over the entire DR watershed.**

277 Figure 5 demonstrates the simulated hydrographs for the four return periods. The upper and lower spread (75<sup>th</sup> and 25<sup>th</sup>  
 278 quantiles) of the hydrograph indicates the range of variability of simulated hydrographs. For the 10-yr return period, the  
 279 hydrograph is relatively smooth with a smaller spread. With increasing return periods, the hydrograph is peakier with a  
 280 shorter duration of high magnitude discharge. The hydrograph for the 50-yr return period shows a transitional shape  
 281 between small (10-yr) and large (100-yr and 200-yr) rainfall return periods. For the 100-yr return period, the upper spread  
 282 shows a tendency toward dual peaks, which cannot be revealed from conventional design flood practices. Since in the  
 283 conventional rainfall flood frequency approach, the design storm is temporally idealized as a unimodal peak process. By  
 284 using these design storms, the flood response is generally simulated as a unimodal peak process. The above results imply  
 285 the uncertainty and insufficiency of flood frequency analysis using the conventional methods. For the 200-yr return period,  
 286 the hydrograph is peakiest with a large upper spread.



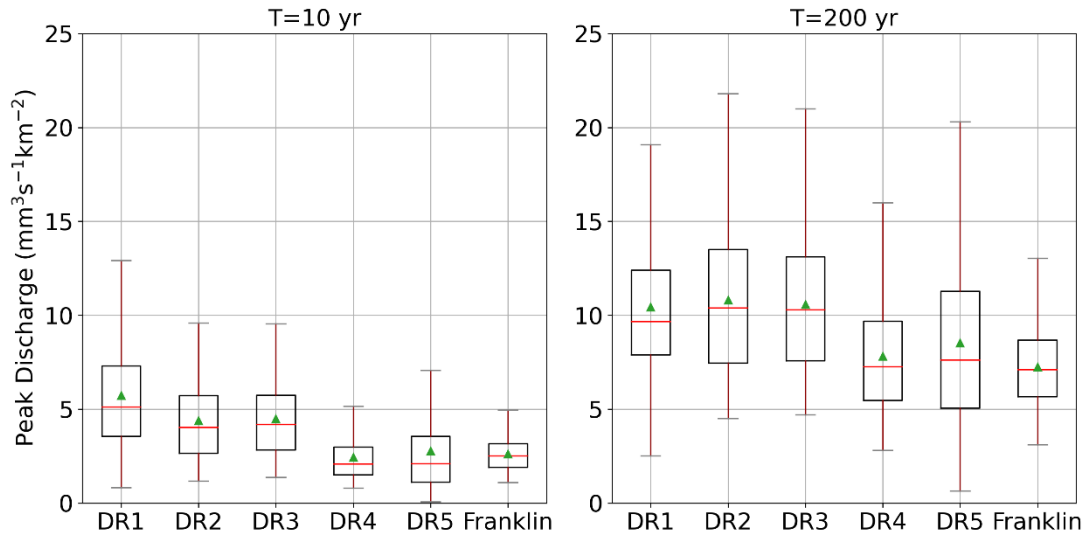
287

288 **Figure 5. Time series of simulated hydrographs for Franklinton based on the 3-h design storms from 10-yr to 200-**  
 289 **yr return periods with spatially uniform (blue) and spatially distributed (red) rainfall. The grey bar indicates the**  
 290 **median value of the basin-averaged rainfall rate.**

291

292 **3.2.2 Spatial distribution of flood magnitude**

293 The distribution of flood peaks over the five subwatersheds exhibits contrasting variation with rainfall return periods  
 294 ranging from 10 to 200 years (Fig. 6). Generally, basin scale plays an important role in determining the distribution of flood  
 295 magnitudes. Under the 10-yr rainfall return period, DR1 and DR2, with similar basin scales of 1.32 and 1.92 km<sup>2</sup>  
 296 respectively, have higher flood peaks and interquartile ranges than other subwatersheds. DR5 (2.05 km<sup>2</sup>) has comparable  
 297 flood magnitude with DR4 (6.3 km<sup>2</sup>) and Franklinton (14.3 km<sup>2</sup>), while has a larger interquartile range than the latter  
 298 two. DR3 with a basin scale of 4.95 km<sup>2</sup>, has comparable flood magnitudes with DR1 and DR2. Under the 200-yr rainfall  
 299 return period, DR2 and DR3 have a slightly larger flood magnitude than DR1. DR5 has the largest interquartile range than  
 300 others, though its flood peaks are smaller than other small watersheds.



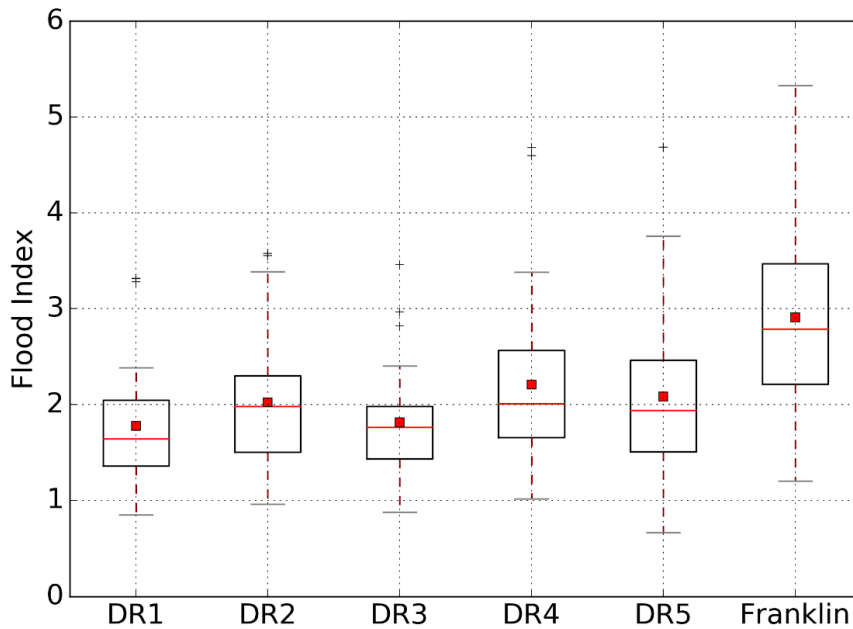
301

302 **Figure 6. Boxplots of normalized flood peaks for Franklinton and five subwatersheds.**

303 Results show that sub-basin flood distributions vary significantly with rainfall return periods. DR1 with 33% larger  
 304 impervious area and more than double the stormwater detention controlled area than DR2 (Table 1), has 26% larger median  
 305 flood peak under small rainfall return period. For large return periods, DR2 has a slightly larger median peak and a larger  
 306 peak and interquartile range than DR1. The contrasting peaks in DR1 and DR2 imply that flood peaks are less impacted by  
 307 impervious areas for extreme storms while for small rainfall events, detention infrastructure may play a less role in the  
 308 detention of flood peaks. DR5, with the smallest detention controlled area, has the smallest flood peaks under small rainfall  
 309 return period. Under large return period, however, it has the largest changes in peak discharges with comparable flood  
 310 peaks with subwatersheds larger than 6 km<sup>2</sup>. DR3 and DR4, with basin scale of 4.95 and 6.29 km<sup>2</sup>, have contrasting flood  
 311 magnitude under small and large return periods. DR3 with larger impervious area and detention controlled area has larger  
 312 flood peaks than DR4. The difference is more significant for small rainfall events with the median value of flood peak for  
 313 DR3 more than double that of DR4. From these results, it implies that impervious area and detention controlled area play  
 314 a significant role in determining the peak discharges, but the impact reduces with increasing rainfall return period. The  
 315 detention infrastructure impacts flood peak and its variability. It should be noted that difficulties remain in attributing  
 316 specific changes in urban flood peak distributions to specific urbanization characteristics (Zhou *et al.*, 2017). The role of  
 317 specific urban features in flood responses is beyond the scope of this paper (see Miller *et al.* (2021) for additional discussion  
 318 based on analyses of Dead Run discharge observations).

319 We further examine the spatial distribution of flood magnitude over the Dead Run watershed under the 100-yr return period  
 320 of flood at Franklinton (Fig. 7). The dimensionless flood index is used to compare flood peak magnitudes over the  
 321 watershed (Lu *et al.*, 2017). The flood index is computed as the maximum flow discharge divided by the computed 10-yr

322 flood ( $Q_{10-y}$ ) at the same location, which is set as the median value of 10-yr peak discharge at the watershed outlet for each  
 323 100-yr design storm simulation. At Franklinton, the flood index and its interquartile range are largest across the  
 324 watersheds, with the median value greater than 2.5. The flood index in the five sub-watersheds is relatively lower, within  
 325 a median value between 1.5 and 2. DR2, as a sub-watershed of DR3, has a larger median value than DR1 and DR3. The  
 326 flood indices at DR1 and DR3 have similar median values and interquartile ranges. Values in DR4 are higher than its sub-  
 327 watershed, DR5, with a median value of 2. The variability of flood magnitudes, indicated by the CV, is stable among the  
 328 watersheds, ranging from 0.30 to 0.39. The spatial distribution of flood magnitude points to the significant heterogeneity  
 329 of flood distributions over the 14.3-km<sup>2</sup> watershed. For storm events that produce the same peak discharge return period at  
 330 the watershed outlet, the subsequent upstream flood response can vary substantially in the Dead Run watershed.



331 **Figure 7. Boxplot of flood index across the DR subwatersheds for the 100-yr design storms.**

333

### 334 3.3 Rainfall-Flood Relationships

#### 335 3.3.1 Rainfall structure and flood response

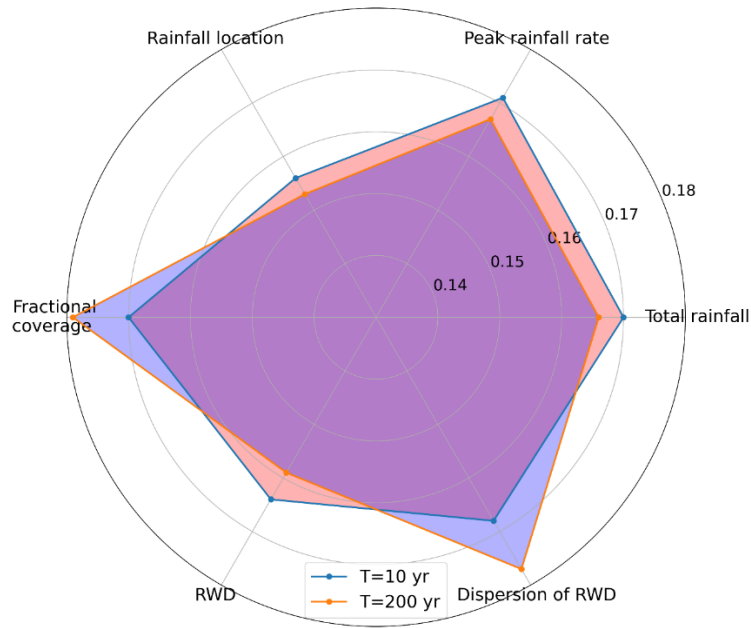
336 We investigate the relationship between the spatial and temporal characteristics of rainfall and flood response for small and  
 337 large rainfall return periods based on Spearman's rank correlation (Fig. A3 in Appendix A). The peak rainfall rate ( $M_{max}$ ),  
 338 total rainfall ( $R_{sum}$ ), fractional coverage ( $Z$ ), rainfall location ( $L$ ), rainfall-weighted flow distance ( $RWD$ ) and the dispersion  
 339 of  $RWD$  ( $S$ ) are used to characterize rainfall spacetime structure. For the 10-yr return period, the flood peak is slightly  
 340 correlated with total rainfall, peak rainfall rate and storm core coverage with correlation coefficient of 0.16. For the 200-yr

341 return period, in contrast, there is no significant correlation between these features with correlation coefficients of -0.09,  
342 0.07 and -0.02, respectively, implying a complex and nonlinear relationship between extreme storms and floods in the  
343 watershed.

344 We used random forest regression models to examine the importance of rainfall characteristics to the flood response.  
345 Random forests (RF) is an ensemble learning method (Breiman, 2001) that aggregates results from multiple models to  
346 achieve better accuracy. RF is one of the most widely-used methods for regression and classification. Moreover, it is  
347 relatively easy to train and test. In this study, rainfall spacetime structure characteristics are used as RF model features. The  
348 flood peak is set as the model target. The relationship between rainfall structure and flood peak is then explored under the  
349 RF-based regression method. The main parameters of the RF model are tuned by a grid search approach (Probst *et al.*,  
350 2019). The prediction performance is assessed using Mean Absolute Error (*MAE*), Root Mean Square Error (*RMSE*), and  
351 explained variance regression score (*E score*) (Achen, 2017). Smaller values of *MAE* and *RMSE* indicate better model  
352 performance. *E score* ranges from 0 to 1 and a larger value indicates a better model (the training process of the RF model  
353 is shown in Fig. A4 in Appendix A).

354 The difference in feature importance is compared between the 10-yr and 200-yr return periods (Fig. 8). For the 10-yr return  
355 period, peak rainfall rate ( $M_{max}$ ) and total rainfall ( $R_{sum}$ ) are the most two important features with feature importance of  
356 0.17. For the 200-yr return period, however, the dispersion of RWD ( $S$ ) and fractional coverage of storm core ( $Z$ ) are more  
357 important than  $M_{max}$  and  $R_{sum}$ . The rainfall location ( $L$ ) has the smallest importance for both return periods. The results  
358 demonstrate the different relationships between rainfall structure and flood response under small and extreme rainfall  
359 events. For extreme storms, the maximum discharge is more closely linked to the spatial structure of rainfall, which is  
360 consistent with the results in Peleg *et al.* (2017); Zhu *et al.* (2018). Though it appears that the difference is moderate, but  
361 for a such small watershed, the tendency of the change of spatiotemporal rainfall feature importance is noteworthy.





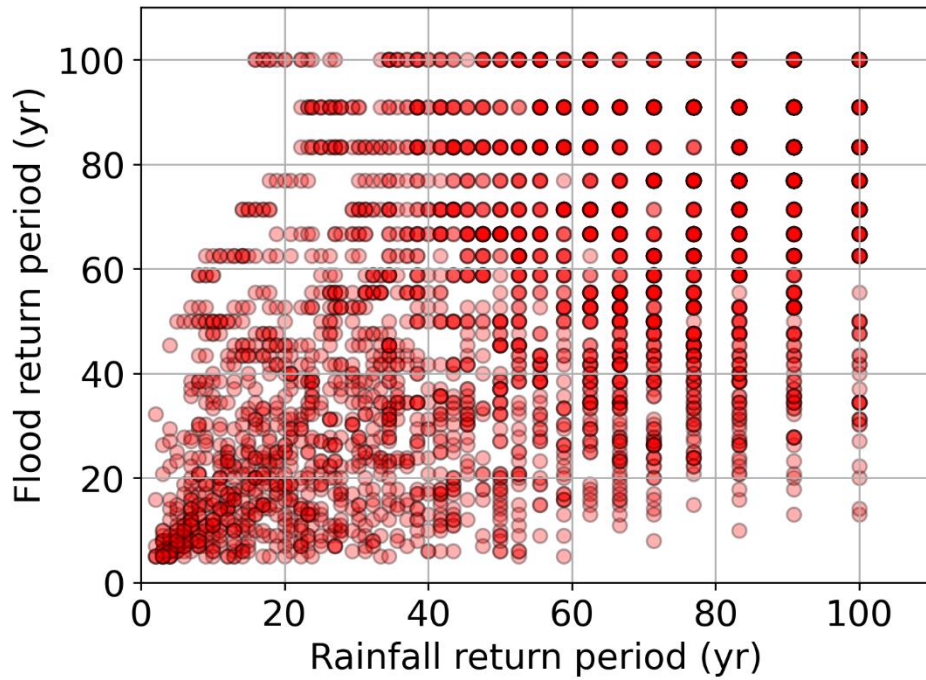
362

363 **Figure 8. Feature importance analysis of RF model for space-time rainfall structure and 10-yr (red) and 200-yr (blue)**  
 364 **flood peaks.**

365

366 **3.3.2 Rainfall return period vs. flood return period**

367 In conventional design storm/flood practices, the return period of rainfall and peak discharge is often assumed to be  
 368 equivalent (Rahman *et al.*, 2002). Under the SST framework, we can examine this assumption (Wright *et al.*, 2014a). At  
 369 the 14.3-km<sup>2</sup> basin scale, for each SST realization containing 100 rainfall scenarios with return period from 5 years up to  
 370 100 years, the peak discharge can be simulated and ordered. Flood frequency for return periods from 5 years up to 100  
 371 years is then estimated from the ordered peaks. We run 30 SST realizations in total. The Spearman's rank correlation of the  
 372 two return periods is 0.5 (Fig. 9). The results quantitatively confirm that the assumption of a 1:1 return period equivalency  
 373 between design storm and design flood cannot hold, even in a small highly-urbanized watershed where drainage network  
 374 and rainfall structure play an important role in flood response. Similar results can be found between subbasins flood and  
 375 DR-scale rainfall return periods (results not shown for the sake of brevity).



376

377 **Figure 9. Scatterplot comparison return periods for rainfall and peak discharge for individual SST-based**  
 378 **simulations.**

379

### 380 3.3.3 Impact of rainfall spatial heterogeneity on flood responses

381 We also compared the simulated flood response resulting when rainfall is uniform over the watershed, rather than spatially  
 382 distributed as in previous analyses (Fig. 4 and Table 2). Generally, flood peaks generated from uniform rainfall have lower  
 383 peaks than from non-uniform rainfall. The difference increases with the return period. Under the 10-yr return period, the  
 384 shapes of the two hydrographs have similar upper and lower bounds (75% and 25% quantiles). The median flood peak  
 385 using non-uniform scenarios is 22% higher than the uniform scenarios. Under the 200-yr return period, the hydrograph  
 386 resulting from non-uniform rainfall is much peakier than the uniform SST scenarios with higher upper and lower bounds.  
 387 The lower bound of hydrograph by non-uniform SST scenarios is close to the median hydrograph of uniform SST scenarios.  
 388 The impact of rainfall spatial heterogeneity among the five subwatersheds is different. DR1, with a basin scale of 1.32 km<sup>2</sup>  
 389 and located in the northwest boundary of the watershed, was the least-impacted by rainfall spatial distribution for all return  
 390 periods. In DR2, on the other hand, which is similar in drainage area to DR1, the flood peak increased by 46% for the 200-  
 391 yr return period. For DR3 and DR4, the spatial heterogeneity of rainfall contributes more to the flood peaks in DR4 than  
 392 in DR3. The most striking difference in flood peaks is in DR5 for the 50-yr return period. The difference in flood magnitude  
 393 is 75%. As mentioned above, DR5 is the sub-basin with the least detention controlled area. This finding is likely tied to the  
 394 complex relationship between space-time rainfall structure and the drainage network. We can thus conclude that the spatial

395 heterogeneity of rainfall can increase flood peaks dramatically under both small and large return periods. The impact  
 396 increases with the return period. This result shows that the assumption of spatially uniform rainfall will underestimate flood  
 397 frequency.

398 **Table 2. The median flood peak reductions using spatially uniform and spatially distributed rainfall.**

	T=10 yr	T=50 yr	T=100 yr	T=200 yr
DR1	14%	20%	13%	26%
DR2	19%	40%	28%	42%
DR3	24%	33%	27%	31%
DR4	32%	51%	38%	35%
DR5	15%	75%	37%	30%
Franklin	22%	36%	31%	42%

399

#### 400 **4. Summary and conclusions**

401 This paper addresses the problem of the impacts of short-duration rainfall variability on hydrologic response in the small  
 402 urbanized watershed. By coupling a high-resolution radar rainfall dataset and stochastic storm transposition (SST) with the  
 403 GSSHA distributed physics-based model (see also (Wright *et al.*, 2014a; Zhu *et al.*, 2018)), the relationships between  
 404 rainfall spatiotemporal structure and urban flood response are examined. The main findings are as follows:

405 1. The flood frequency distributions for subwatersheds within the highly-urbanized 14.3-km<sup>2</sup> Dead Run watershed  
 406 demonstrate the complexities of flood response for both short and long rainfall return periods. For 3-h extreme storms, the  
 407 large variability of flood magnitude shows a pronounced role of rainfall space-time structure in flood production. This calls  
 408 into question the common design storm assumption of spatially uniform rainfall. The response time is less affected by  
 409 rainfall structure and appears to be more closely associated with the basin scale and drainage network features.

410 2. The spatial heterogeneity of flood frequency over the 14.3-km<sup>2</sup> watershed is striking for the 100-yr return period. The  
 411 intercomparison between subwatersheds shows that the impact of impervious area decreases with increasing return periods.  
 412 For the 100-yr return period, storm events that produce the same peak discharge return period at the basin outlet can be the  
 413 result of very different upstream flood responses even in a small-scale watershed.

414 3. The relationship between the spacetime structure of rainfall and flood response is complex. For smaller and more frequent  
 415 rainfall events, flood peaks are more closely linked to the temporal features of rainfall (total rainfall and peak rainfall rate).  
 416 For extreme storms, the maximum discharge is closely linked to the spatial structure of rainfall (storm core coverage). This  
 417 finding is broadly consistent with Peleg *et al.* (2017) and Zhu *et al.* (2018), despite the very different drainage scales

418 considered in those studies. There is no significant correlation between rainfall peak, total rainfall and flood peaks, implying  
419 an important role of surface properties in urbanized watersheds. Similar to Wright *et al.* (2014a), this comparison calls into  
420 question the conventional design storm assumption of a 1:1 equivalency between rainfall and flood peak return periods.

421 4. The spatial heterogeneity of rainfall is a key driver of flood response across scales. Relative to spatially uniform rainfall,  
422 spatially distributed rainfall can increase flood peaks by 50% on average at the watershed outlet and its subwatersheds for  
423 both small and large return periods. This finding is broadly consistent with prior results at much larger scales in an  
424 agricultural setting Zhu *et al.* (2018) and suggests both spatial and temporal rainfall distributions need to be considered in  
425 flood frequency analyses, even in relatively small urban watersheds. This study also implies that the drainage network  
426 substantially alters the impact of rainfall characteristics on runoff.

427 Coupling the GSSHA model and SST-based rainfall frequency analysis, this study provides an effective approach for  
428 regional flood frequency analysis for urban watersheds. Some idealized assumptions used in conventional methods are  
429 questioned. The approach can be used to explore the dominant control on the upper tail of urban flood peaks, without many  
430 of the limiting assumptions associated with design storm methods. The study area could be extended in future work with  
431 larger basin scales and by manipulating the spatial heterogeneity of basin characteristics within GSSHA or other similar  
432 modeling systems.

#### 433 **Acknowledgments**

434 This study was supported by the National Science Foundation of China (Grant 51909191 and Grant 52111530045) and the  
435 US National Science Foundation (CBET-1444758).

#### 436 **Data availability**

437 Radar data are archived at Princeton University and can be downloaded from the url  
438 <http://arks.princeton.edu/ark:/88435/dsp01q524jr55d>.

#### 440 **Author contributions**

441 The main contributions from each co-author are as follows. Zhengzheng Zhou contributed to the computation and  
442 organization of the paper. James A. Smith contributed to the supervision and writing. Mary Lynn Beack is responsible for  
443 generating the radar rainfall data. Brianne K. Smith contributed to the construction of the initial hydrological model. Daniel  
444 B. Wright contributed to the writing of the paper. Shuguang Liu contributed to the supervision and writing.

445

446 **Competing interests**

447 The authors declare that they have no conflict of interest.

448

449 **Reference**

- 450 Achen, C. H. (2017), What Does “Explained Variance“ Explain?: Reply, *Political Analysis*, 2, 173-184.  
451 doi:10.1093/pan/2.1.173
- 452 Adams, R., A. W. Western, and A. W. Seed (2012), An analysis of the impact of spatial variability in rainfall on runoff and  
453 sediment predictions from a distributed model, *Hydrological Processes*, 26(21), 3263-3280. doi:10.1002/hyp.8435
- 454 Beighley, R. E., and G. E. Moglen (2002), Trend Assessment in Rainfall-Runoff Behavior in Urbanizing Watersheds,  
455 *Journal of Hydrologic Engineering*, 7(1), 27-34. doi:10.1061/(ASCE)1084-0699(2002)7:1(27)
- 456 Berne, A., G. Delrieu, J.-D. Creutin, and C. Obled (2004), Temporal and spatial resolution of rainfall measurements  
457 required for urban hydrology, *Journal of Hydrology*, 299(3), 166-179. doi:10.1016/j.jhydrol.2004.08.002
- 458 Breiman, L. (2001), Random Forests, *Machine Learning*, 45(1), 5-32. 10.1023/a:1010933404324
- 459 Bruni, G., R. Reinoso, d. G. Van, N. C., F. H. L. R. Clemens, and J. A. E. Ten Veldhuis (2015), On the sensitivity of urban  
460 hydrodynamic modelling to rainfall spatial and temporal resolution, *Hydrology and Earth System Sciences*, 19(2), 691-709.  
461 doi:10.5194/hess-19-691-2015, 2015
- 462 Cristiano, E., M. C. ten Veldhuis, and N. van de Giesen (2017), Spatial and temporal variability of rainfall and their effects  
463 on hydrological response in urban areas – a review, *Hydrology and Earth System Sciences*, 21(7), 3859-3878.  
464 doi:10.5194/hess-21-3859-2017
- 465 Cristiano, E., M. C. ten Veldhuis, S. Gaitan, S. Ochoa Rodriguez, and N. van de Giesen (2018), Critical scales to explain  
466 urban hydrological response: an application in Cranbrook, London, *Hydrol. Earth Syst. Sci.*, 22(4), 2425-2447.  
467 doi:10.5194/hess-22-2425-2018
- 468 Cristiano, E., M.-c. ten Veldhuis, D. B. Wright, J. A. Smith, and N. van de Giesen (2019), The Influence of Rainfall and  
469 Catchment Critical Scales on Urban Hydrological Response Sensitivity, *Water Resources Research*, 55(4), 3375-3390.  
470 doi:10.1029/2018WR024143
- 471 Downer, C. W., and F. L. Ogden (2004), GSSHA: Model to simulate diverse stream flow producing processes, *Journal of*  
472 *Hydrologic Engineering*, 9(3), 161-174. doi:10.1061/(ASCE)1084-0699(2004)9:3(161)
- 473 Downer, C. W., and F. L. Ogden (2006), Gridded Surface Subsurface Hydrologic Analysis (GSSHA) User's Manual;  
474 Version 1.43 for Watershed Modeling System 6.1.
- 475 Emmanuel, I., H. Andrieu, E. Leblois, and B. Flahaut (2012), Temporal and spatial variability of rainfall at the urban  
476 hydrological scale, *Journal of Hydrology*, 430-431, 162-172. doi:10.1016/j.jhydrol.2012.02.013
- 477 Emmanuel, I., H. Andrieu, E. Leblois, N. Janey, and O. Payrastra (2015), Influence of rainfall spatial variability on rainfall–  
478 runoff modelling: Benefit of a simulation approach?, *Journal of Hydrology*, 531, 337-348.  
479 doi:10.1016/j.jhydrol.2015.04.058
- 480 Faurès, J.-M., D. C. Goodrich, D. A. Woolhiser, and S. Sorooshian (1995), Impact of small-scale spatial rainfall variability  
481 on runoff modeling, *Journal of Hydrology*, 173(1), 309-326. doi:10.1016/0022-1694(95)02704-S
- 482 Fulton, R. A., J. P. Breidenbach, D.-J. Seo, D. A. Miller, and T. O'Bannon (1998), The WSR-88D rainfall algorithm,  
483 *Weather and Forecasting*, 13(2), 377-395. doi:10.1175/1520-0434(1998)013<0377:TWRA>2.0.CO;2
- 484 Galster, J. C., F. J. Pazzaglia, B. R. Hargreaves, D. P. Morris, S. C. Peters, and R. N. Weisman (2006), Effects of urbanization  
485 on watershed hydrology: The scaling of discharge with drainage area, *Geology*, 34(9), 713-716. doi:10.1130/g22633.1
- 486 Gebremichael, M., and W. F. Krajewski (2004), Assessment of the statistical characterization of small-scale rainfall

487 variability from radar: Analysis of TRMM ground validation datasets, *Journal of Applied Meteorology*, 43(8), 1180-1199.  
488 doi:10.1175/1520-0450(2004)043<1180:AOTSCO>2.0.CO;2

489 Gesch, D. B., M. J. Oimoen, S. K. Greenlee, C. A. Nelson, M. J. Steuck, and D. J. Tyler (2002), The national elevation data  
490 set, *Photogrammetric Engineering and Remote Sensing*, 68(1), 5-11.

491 Gourley, J. J., et al. (2017), The FLASH Project: Improving the Tools for Flash Flood Monitoring and Prediction across  
492 the United States, *Bulletin of the American Meteorological Society*, 98(2), 361-372. doi:10.1175/bams-d-15-00247.1

493 Krajewski, W., and J. Smith (2002), Radar hydrology: rainfall estimation, *Advances in water resources*, 25(8-12), 1387-  
494 1394. doi:10.1016/S0309-1708(02)00062-3

495 Krajewski, W. F., A. Kruger, J. A. Smith, R. Lawrence, C. Gunyon, R. Goska, B.-C. Seo, P. Domaszczynski, M. L. Baeck,  
496 and M. K. Ramamurthy (2011), Towards better utilization of NEXRAD data in hydrology: an overview of Hydro-  
497 NEXRAD, *Journal of hydroinformatics*, 13(2), 255-266. doi:10.2166/hydro.2010.056

498 Lin, N., J. A. Smith, G. Villarini, T. P. Marchok, and M. L. Baeck (2010), Modeling extreme rainfall, winds, and surge from  
499 Hurricane Isabel (2003), *Weather and forecasting*, 25(5), 1342-1361. doi:10.1175/2010WAF2222349.1

500 Lindner, G. A., and A. J. Miller (2012), Numerical modeling of stage-discharge relationships in urban streams, *Journal of*  
501 *Hydrologic Engineering*, 17(4), 590-596.

502 Lu, P., J. A. Smith, and N. Lin (2017), Spatial Characterization of Flood Magnitudes over the Drainage Network of the  
503 Delaware River Basin, *Journal of Hydrometeorology*, 18(4), 957-976. doi:10.1175/jhm-d-16-0071.1

504 Maryland, S. o. (1982), Department of the Environment : Water management, stormwater management.

505 Meierdiercks, K. L., J. A. Smith, M. L. Baeck, and A. J. Miller (2010), Analyses of urban drainage network structure and  
506 its impact on hydrologic response, *JAWRA Journal of the American Water Resources Association*, 46(5), 932-943.

507 Miller, A. J., C. Welty, J. M. Duncan, M. L. Baeck, and J. A. Smith (2021), Assessing urban rainfall-runoff response to  
508 stormwater management extent, *Hydrological Processes*, 35(7), e14287. <https://doi.org/10.1002/hyp.14287>

509 Moreau, E., J. Testud, and E. Le Bouar (2009), Rainfall spatial variability observed by X-band weather radar and its  
510 implication for the accuracy of rainfall estimates, *Advances in Water Resources*, 32(7), 1011-1019.  
511 doi:10.1016/j.advwatres.2008.11.007

512 Morin, E., D. C. Goodrich, R. A. Maddox, X. Gao, H. V. Gupta, and S. Sorooshian (2006), Spatial patterns in thunderstorm  
513 rainfall events and their coupling with watershed hydrological response, *Advances in Water Resources*, 29(6), 843-860.

514 Nash, J. E., and J. V. Sutcliffe (1970), River flow forecasting through conceptual models part I — A discussion of principles,  
515 *Journal of Hydrology*, 10(3), 282-290. [https://doi.org/10.1016/0022-1694\(70\)90255-6](https://doi.org/10.1016/0022-1694(70)90255-6)

516 Nelson, P. A., J. A. Smith, and A. J. Miller (2006), Evolution of channel morphology and hydrologic response in an  
517 urbanizing drainage basin, *Earth Surface Processes and Landforms*, 31(9), 1063-1079. doi:10.1002/esp.1308

518 Nikolopoulos, E. I., M. Borga, D. Zoccatelli, and E. N. Anagnostou (2014), Catchment-scale storm velocity: Quantification,  
519 scale dependence and effect on flood response, *Hydrological Sciences Journal*, 59(7), 1363-1376.  
520 doi:10.1080/02626667.2014.923889

521 Ntelekos, A. A., J. A. Smith, M. L. Baeck, W. F. Krajewski, A. J. Miller, and R. Goska (2008), Extreme hydrometeorological  
522 events and the urban environment: Dissecting the 7 July 2004 thunderstorm over the Baltimore MD Metropolitan Region,  
523 *Water Resources Research*, 44(8), 1-19. doi:10.1029/2007WR006346

524 Ochoa-Rodriguez, S., L.-P. Wang, A. Gires, R. D. Pina, R. Reinoso-Rondinel, G. Bruni, A. Ichiba, S. Gaitan, E. Cristiano,  
525 and J. van Assel (2015), Impact of spatial and temporal resolution of rainfall inputs on urban hydrodynamic modelling  
526 outputs: A multi-catchment investigation, *Journal of Hydrology*, 531(2), 389-407. doi:10.1016/j.jhydrol.2015.05.035

527 Ogden, F. L., N. Raj Pradhan, C. W. Downer, and J. A. Zahner (2011), Relative importance of impervious area, drainage  
528 density, width function, and subsurface storm drainage on flood runoff from an urbanized catchment, *Water Resources*  
529 *Research*, 47(12). doi:10.1029/2011wr010550

530 Paschalis, A., S. Fatichi, P. Molnar, S. Rimkus, and P. Burlando (2014), On the effects of small scale space–time variability

531 of rainfall on basin flood response, *Journal of Hydrology*, 514, 313-327. doi:10.1016/j.jhydrol.2014.04.014

532 Peleg, N., F. Blumensaat, P. Molnar, S. Fatichi, and P. Burlando (2017), Partitioning the impacts of spatial and

533 climatological rainfall variability in urban drainage modeling, *Hydrology and Earth System Sciences*, 21(3), 1559.

534 doi:10.5194/hess-21-1559-2017

535 Perez, G., R. Mantilla, W. F. Krajewski, and D. B. Wright (2019), Using Physically Based Synthetic Peak Flows to Assess

536 Local and Regional Flood Frequency Analysis Methods, *Water Resources Research*, 55(11), 8384-8403.

537 doi:10.1029/2019WR024827

538 Pickett, S. T. A., and M. L. Cadenasso (2006), Advancing urban ecological studies: Frameworks, concepts, and results from

539 the Baltimore Ecosystem Study, *Austral Ecology*, 31(2), 114-125. doi:10.1111/j.1442-9993.2006.01586.x

540 Probst, P., M. N. Wright, and A. L. Boulesteix (2019), Hyperparameters and tuning strategies for random forest, *Wiley*

541 *Interdisciplinary Reviews: Data Mining and Knowledge Discovery*, 9(3), e1301. doi:10.1002/widm.1301

542 Rafieeinasab, A., A. Norouzi, S. Kim, H. Habibi, B. Nazari, D.-J. Seo, H. Lee, B. Cosgrove, and Z. Cui (2015), Toward

543 high-resolution flash flood prediction in large urban areas – Analysis of sensitivity to spatiotemporal resolution of rainfall

544 input and hydrologic modeling, *Journal of Hydrology*, 531, 370-388. doi:10.1016/j.jhydrol.2015.08.045

545 Rahman, A., P. E. Weinmann, T. M. T. Hoang, and E. M. Laurenson (2002), Monte Carlo simulation of flood frequency

546 curves from rainfall, *Journal of Hydrology*, 256(3), 196-210. doi:10.1016/S0022-1694(01)00533-9

547 Saghafian, B., P. Y. Julien, and F. L. Ogden (1995), Similarity in catchment response: 1. Stationary rainstorms, *Water*

548 *Resources Research*, 31(6), 1533-1541. doi:10.1029/95WR00518

549 Schellart, A. N. A., W. J. Shepherd, and A. J. Saul (2012), Influence of rainfall estimation error and spatial variability on

550 sewer flow prediction at a small urban scale, *Advances in Water Resources*, 45, 65-75. doi:10.1016/j.advwatres.2011.10.012

551 Seo, B.-C., W. F. Krajewski, A. Kruger, P. Domaszczynski, J. A. Smith, and M. Steiner (2011), Radar-rainfall estimation

552 algorithms of Hydro-NEXRAD, *Journal of Hydroinformatics*, 13(2), 277-291. doi:10.2166/hydro.2010.003

553 Sharif, H. O., A. A. Hassan, S. Bin-Shafique, H. Xie, and J. Zeitler (2010), Hydrologic modeling of an extreme flood in

554 the Guadalupe River in Texas, *JAWRA Journal of the American Water Resources Association*, 46(5), 881-891.

555 doi:10.1111/j.1752-1688.2010.00459.x

556 Sharif, H. O., S. Chintalapudi, A. A. Hassan, H. Xie, and J. Zeitler (2013), Physically Based Hydrological Modeling of the

557 2002 Floods in San Antonio, Texas, *Journal of Hydrologic Engineering*, 18(2), 228-236. doi:10.1061/(ASCE)HE.1943-

558 5584.0000475

559 Smith, B., J. Smith, M. Baeck, and A. Miller (2015), Exploring storage and runoff generation processes for urban flooding

560 through a physically based watershed model, *Water Resources Research*, 51(3), 1552-1569. doi:10.1002/2014WR016085

561 Smith, B. K., J. A. Smith, M. L. Baeck, G. Villarini, and D. B. Wright (2013), Spectrum of storm event hydrologic response

562 in urban watersheds, *Water Resources Research*, 49(5), 2649-2663. doi:10.1002/wrcr.20223

563 Smith, J. A., and W. F. Krajewski (1991), Estimation of the mean field bias of radar rainfall estimates, *Journal of Applied*

564 *Meteorology*, 30(4), 397-412.

565 Smith, J. A., M. L. Baeck, K. L. Meierdiercks, A. J. Miller, and W. F. Krajewski (2007), Radar rainfall estimation for flash

566 flood forecasting in small urban watersheds, *Advances in Water Resources*, 30(10), 2087-2097.

567 doi:10.1016/j.advwatres.2006.09.007

568 Smith, J. A., M. L. Baeck, J. E. Morrison, P. Sturdevant-Rees, D. F. Turner-Gillespie, and P. D. Bates (2002), The regional

569 hydrology of extreme floods in an urbanizing drainage basin, *Journal of Hydrometeorology*, 3(3), 267-282.

570 doi:10.1175/1525-7541(2002)003<0267:TRHOEF>2.0.CO;2

571 Smith, J. A., A. J. Miller, M. L. Baeck, P. A. Nelson, G. T. Fisher, and K. L. Meierdiercks (2005a), Extraordinary Flood

572 Response of a Small Urban Watershed to Short-Duration Convective Rainfall, *Journal of Hydrometeorology*, 6(5), 599-

573 617. doi:10.1175/JHM426.1

574 Smith, J. A., M. L. Baeck, K. L. Meierdiercks, P. A. Nelson, A. J. Miller, and E. J. Holland (2005b), Field studies of the

575 storm event hydrologic response in an urbanizing watershed, *Water Resources Research*, 41(10), W10413(10415).  
576 doi:10.1029/2004wr003712

577 Smith, J. A., M. L. Baeck, G. Villarini, C. Welty, A. J. Miller, and W. F. Krajewski (2012), Analyses of a long-term, high-  
578 resolution radar rainfall data set for the Baltimore metropolitan region, *Water Resources Research*, 48(4), 1-14.  
579 doi:10.1029/2011wr010641

580 ten Veldhuis, M. C., Z. Zhou, L. Yang, S. Liu, and J. Smith (2018), The role of storm scale, position and movement in  
581 controlling urban flood response, *Hydrology and Earth System Sciences*, 22(1), 417-436. 10.5194/hess-22-417-2018

582 Wright, D. B., J. A. Smith, and M. L. Baeck (2014a), Flood frequency analysis using radar rainfall fields and stochastic  
583 storm transposition, *Water Resources Research*, 50(2), 1592-1615. doi:10.1002/2013WR014224

584 Wright, D. B., R. Mantilla, and C. D. Peters-Lidard (2017), A remote sensing-based tool for assessing rainfall-driven  
585 hazards, *Environmental Modelling & Software*, 90, 34-54. doi:10.1016/j.envsoft.2016.12.006

586 Wright, D. B., G. Yu, and J. F. England (2020), Six decades of rainfall and flood frequency analysis using stochastic storm  
587 transposition: Review, progress, and prospects, *Journal of Hydrology*, 585, 124816. doi:10.1016/j.jhydrol.2020.124816

588 Wright, D. B., J. A. Smith, G. Villarini, and M. L. Baeck (2012), Hydroclimatology of flash flooding in Atlanta, *Water*  
589 *Resources Research*, 48(4). <https://doi.org/10.1029/2011wr011371>

590 Wright, D. B., J. A. Smith, G. Villarini, and M. L. Baeck (2013), Estimating the frequency of extreme rainfall using weather  
591 radar and stochastic storm transposition, *Journal of Hydrology*, 488, 150-165. doi:10.1016/j.jhydrol.2013.03.003

592 Wright, D. B., J. A. Smith, G. Villarini, and M. L. Baeck (2014b), Long-term high-resolution radar rainfall fields for urban  
593 hydrology, *Journal of the American Water Resources Association*, 50(3), 713-734. doi:10.1111/jawr.12139

594 Yang, L., J. A. Smith, M. L. Baeck, and Y. Zhang (2016), Flash flooding in small urban watersheds: Storm event hydrologic  
595 response, *Water Resources Research*, doi:doi:10.1002/2015WR018326. doi:10.1002/2015WR018326

596 Yang, Y., L. Sun, R. Li, J. Yin, and D. Yu (2020), Linking a Storm Water Management Model to a Novel Two-Dimensional  
597 Model for Urban Pluvial Flood Modeling, *International Journal of Disaster Risk Science*, 11(4), 508-518. 10.1007/s13753-  
598 020-00278-7

599 Yin, J., D. Yu, Z. Yin, M. Liu, and Q. He (2016), Evaluating the impact and risk of pluvial flash flood on intra-urban road  
600 network: A case study in the city center of Shanghai, China, *Journal of Hydrology*, 537, 138-145.  
601 <https://doi.org/10.1016/j.jhydrol.2016.03.037>

602 Yu, G., D. B. Wright, Z. Zhu, C. Smith, and K. D. Holman (2019), Process-based flood frequency analysis in an agricultural  
603 watershed exhibiting nonstationary flood seasonality, *Hydrol. Earth Syst. Sci.*, 23(5), 2225-2243. doi:10.5194/hess-23-  
604 2225-2019

605 Zhou, Z., J. A. Smith, D. B. Wright, M. L. Baeck, and S. Liu (2019), Storm catalog-based analysis of rainfall heterogeneity  
606 and frequency in a complex terrain, *Water Resources Research*, 55(3), 1871-1889. doi:10.1029/2018WR023567

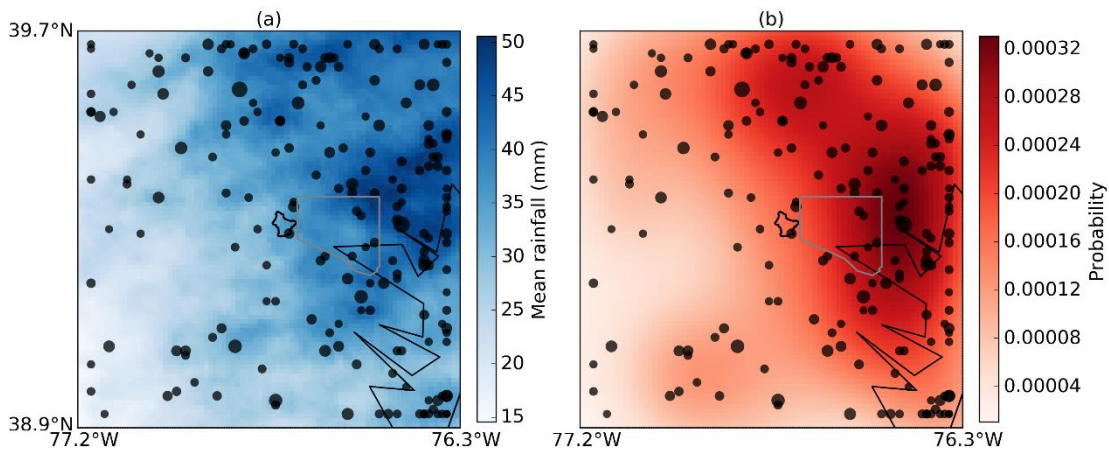
607 Zhou, Z., J. A. Smith, L. Yang, M. L. Baeck, M. Chaney, M.-C. Ten Veldhuis, H. Deng, and S. Liu (2017), The complexities  
608 of urban flood response: Flood frequency analyses for the Charlotte Metropolitan Region, *Water Resources Research*, 53(8),  
609 7401-7425. doi:10.1002/2016WR019997

610 Zhu, Z., D. B. Wright, and G. Yu (2018), The Impact of Rainfall Space-Time Structure in Flood Frequency Analysis, *Water*  
611 *Resources Research*, 54(11), 8983-8998. doi:10.1029/2018wr023550

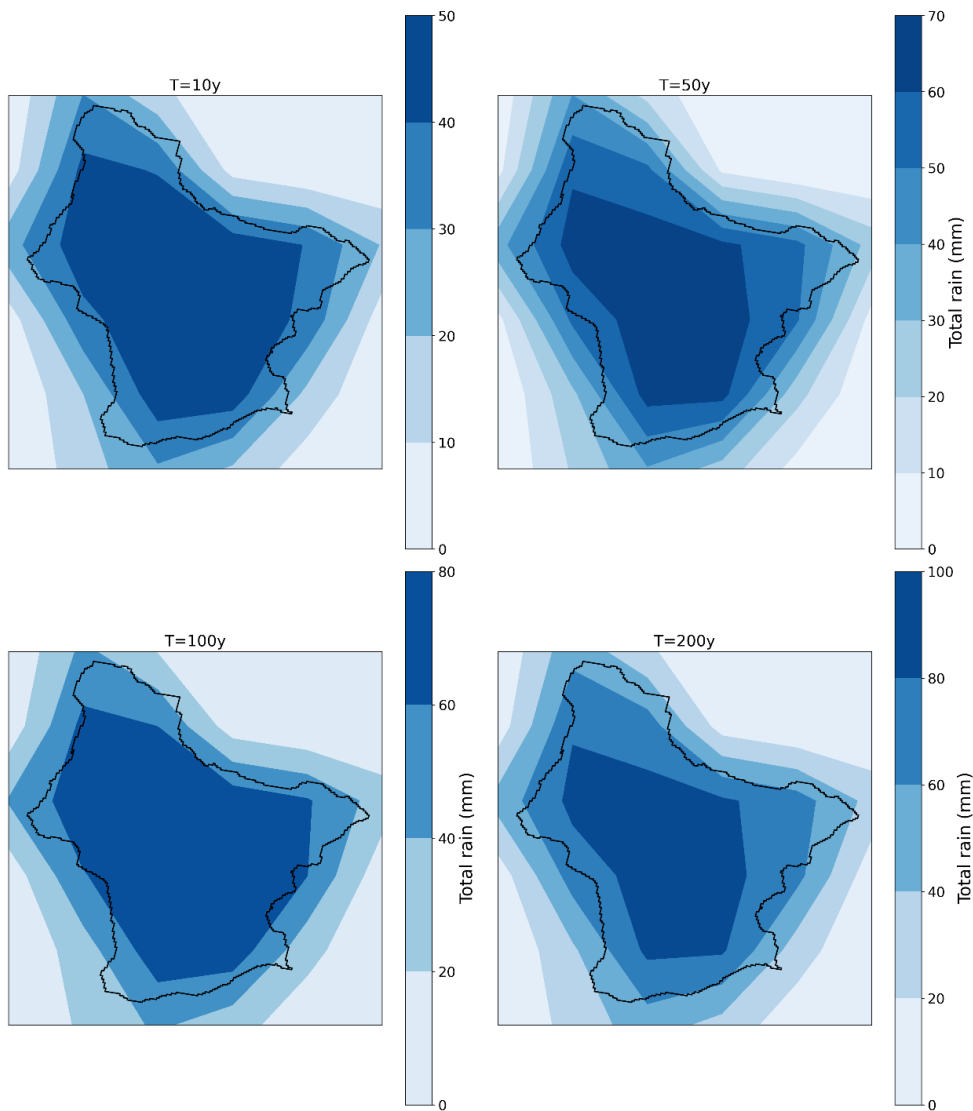
612 Zoccatelli, D., M. Borga, A. Viglione, G. B. Chirico, and G. Blöschl (2011), Spatial moments of catchment rainfall: rainfall  
613 spatial organisation, basin morphology, and flood response, *Hydrology and Earth System Sciences*, 15(12), 3767-3783.  
614 10.5194/hess-15-3767-2011

615  
616  
617  
618



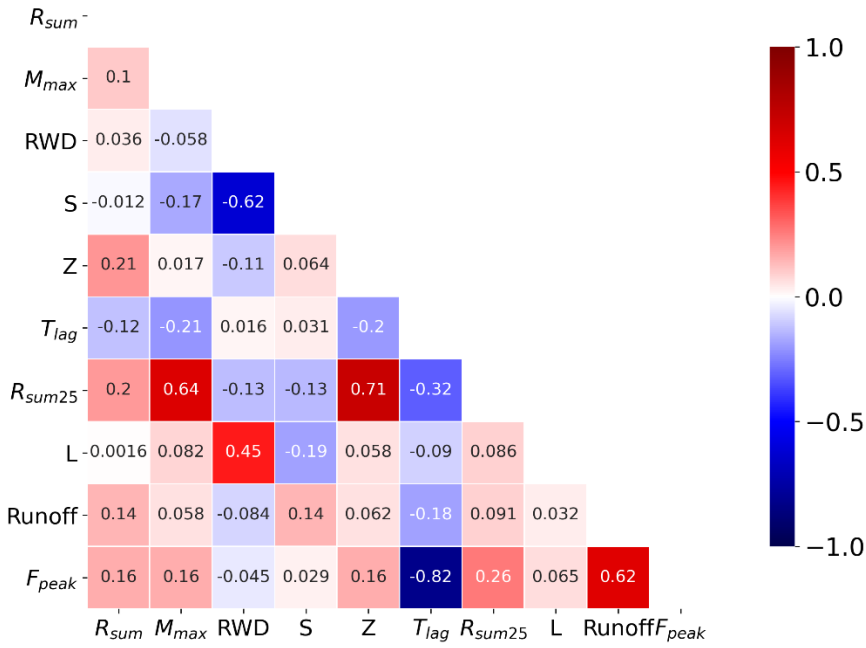


620  
621 Figure A1: Maps of mean storm total rainfall (a) and probability of storm occurrence (b) for the 200 storms in the 3-h  
622 storm catalog (The black dot indicates the location of rainfall centroid).  
623

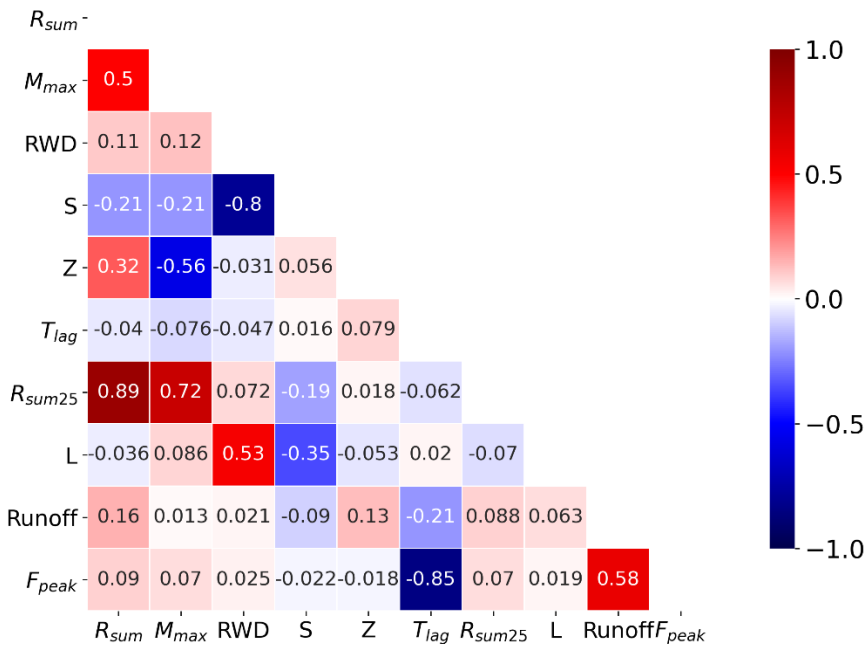


624  
625 Figure A2: Composite map of rainfall distribution for the 10-y, 50-y, 100-y and 200-y return periods.

T=10 yr



T=200 yr



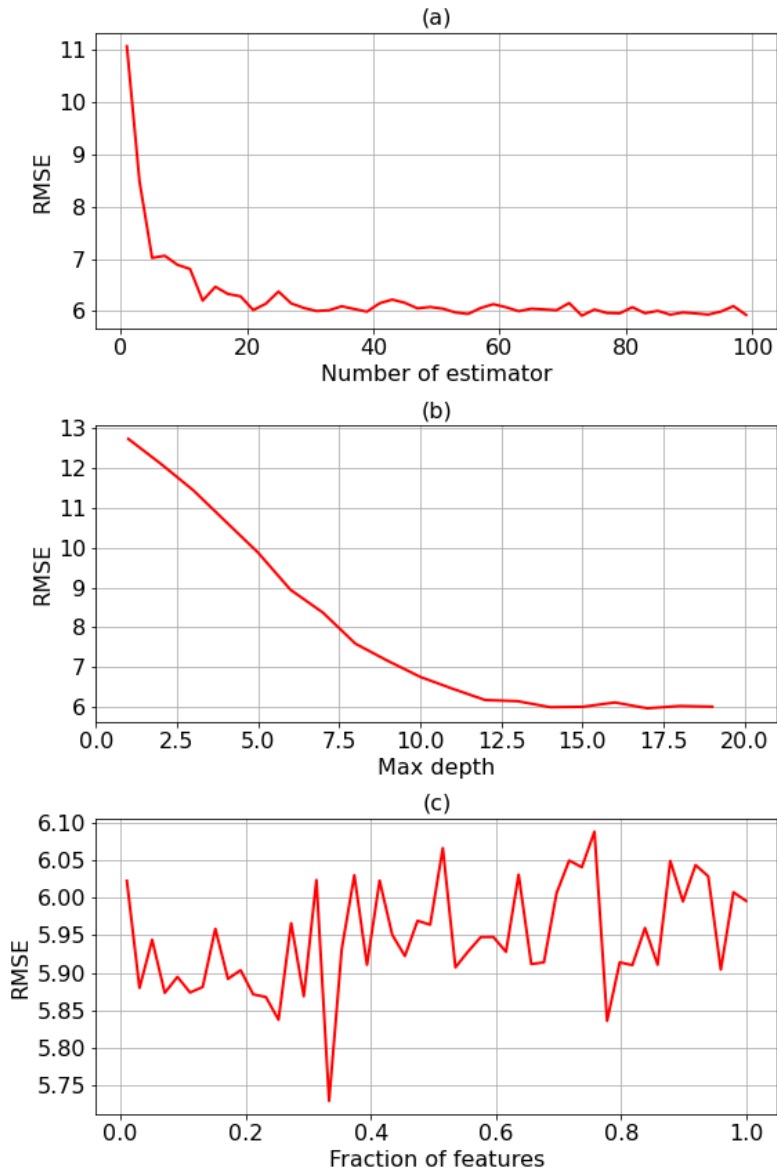
626

627

628

629

Figure A3: Correlation between space-time rainfall structure and flood responses at Franklinton under 10-yr and 200-yr return periods.



630  
 631 Figure A4: The parameter tuning process of RF model (use *RMSE* for example)  
 632